Adaptable by design

encoding complex deformation profiles in mckibben artificial muscles

Kortman, Vera Gesina; Jovanova, Jovana; Sakes, Aimée

DOI
10.1016/j.matdes.2025.115188

Publication date
2025

Document Version
Final published version

Published in
Materials and Design

Citation (APA)
Kortman, V. G., Jovanova, J., & Sakes, A. (2025). Adaptable by design: encoding complex deformation profiles in mckibben artificial muscles. *Materials and Design*, *260*, Article 115188. https://doi.org/10.1016/j.matdes.2025.115188

Materials & Design 260 (2025) 115188

Contents lists available at ScienceDirect

Materials & Design

journal homepage: www.elsevier.com/locate/matdes

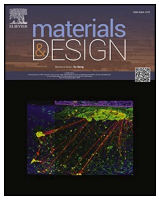

Adaptable by design: encoding complex deformation profiles in mckibben artificial muscles☆

Vera Gesina Kortman [a,*], Jovana Jovanova [b], Aimée Sakes [c]

[a] Department of Maritime and Transport Technology, Department of BioMechanical Engineering, Delft University of Technology, Delft 2628 CD, the Netherlands
[b] Department of Maritime and Transport Technology, Delft University of Technology, Delft 2628 CD, the Netherlands
[c] Department of BioMechanical Engineering, Delft University of Technology, Delft 2628 CD, the Netherlands

ARTICLE INFO

Keywords:
Soft robotics
Bio-inspired design
Actuator
Pneumatic muscle
Embodied intelligence

ABSTRACT

The octopus achieves intricate arm deformations through local muscle interactions rather than centralized coordination. Inspired by this principle, this study aims to develop embodied intelligent McKibben Artificial Muscles (AMs), in which global deformation is encoded directly into their physical structure.

The key design parameter explored is the braiding angle, which governs the type and magnitude of motion. By spatially varying this angle along the actuator, we demonstrate embedded capabilities for local extension and contraction within a single AM. Additionally, a mismatch in braiding angles between opposing wire sets generates a twisting motion. To implement these variations, traditional braiding techniques were adapted for localized angle control. Within a single McKibben AM, a maximum strain of +0.06 and minimum strain of −0.19 was measured. A twist angle of 100° was achieved using a 50.4° angle difference at 50 kPa actuation pressure. A final modular prototype demonstrated the integration of multiple motion modes within a single actuator body.

These results highlight the potential of mechanically intelligent AMs to simplify actuation systems in soft robotics. Applications include wearable technologies such as exoskeletons and prosthetics, as well as bioinspired systems like artificial hearts or continuum robotic arms, where compact and adaptive actuation is essential.

1. Introduction

Nature demonstrates that complex motion does not always require complex control. For example, the octopus achieves intricate arm deformations through local muscle interactions without requiring centralized control. Here, main motions as contraction, extension, bending and twisting are driven by the interplay of longitudinal, circular, and helical muscles. Similar fiber-reinforced architectures are found across a wide range of biological systems, including other muscular hydrostats like squid tentacles and elephant trunks, as well as plant structures. This highlights the widespread relevance of this principle.

In the field of soft robotics, McKibben Artificial Muscles (AMs) are commonly used to achieve similar adaptive characteristics as found in biological systems. These actuators are valued for their compliance, large blocked forces, high contraction ratios and fast response time. McKibben AMs stand out by their design simplicity, consisting of a simple inner bladder wrapped in a braided sleeve, as shown in Fig. 1A. The distal end of the muscle is closed off by an end cap, while the proximal end is connected to a pressure source. The McKibben AM can be either pneumatically or hydraulically actuated by pressurizing the inner bladder. Comparable to the octopus, the motion of the AM is defined by the constraints of directional fibers. Upon pressurization, the inner bladder increases volume, resulting in a diameter expansion. The braided sleeve constrains this radial deformation. Consequently, due to the rotation of its wires, the sleeve transforms the AM's radial deformation into either a contraction or an extension movement. Their similarity to muscles in nature makes these AMs particularly suitable in cases where adaptivity and safety are needed for interaction with humans, such as prosthetics, soft wearables or robotic rehabilitation. They are also advantageous in scenarios that require simple and lightweight control, including continuum robotics.

The design of the braided sleeve is key in determining the McKibben AMs deformation profile. Eq. (1) shows how the generated force of the McKibben AM (F_{muscle}) relates to its diameter D, applied pressure P, strain ε and braiding angle θ_B [1,2]. The braiding angle between the

☆ This article is part of a special issue entitled: 'Soft Robotics' published in Materials & Design.

* Corresponding author.
E-mail addresses: v.g.kortman@tudelft.nl (V.G. Kortman), j.jovanova@tudelft.nl (J. Jovanova), a.sakes@tudelft.nl (A. Sakes).

https://doi.org/10.1016/j.matdes.2025.115188
Received 31 July 2025; Received in revised form 29 October 2025; Accepted 20 November 2025
Available online 21 November 2025

wires of the braided sleeve defines whether F_{muscle} is positive or negative, resulting in either contraction or extension of the AM. These AMs are typically employed as linear actuators.

$$F_{muscle} = \frac{\pi}{4} D^2 P \left(\frac{1}{sin\theta_B} \right)^2 \left\{ 3(1-\varepsilon)^2 cos^2\theta_B - 1 \right\} \quad (1)$$

However, to achieve more complex motions such as bending [3–5], twisting [6–8] or caterpillar-like locomotion [9,10], multiple AM's need to be combined (Fig. 1B). Unlike their counterparts in nature, these combined McKibben AMs have the disadvantage that their implementation often require complex control algorithms or intricate actuation systems to achieve desired complex shape changes. Every individual AM requires a cumbersome system of compressors/pumps, tubing and water/gas containers. The added weight and volume to the robotic system make these McKibben AMs impractical for use in constrained situations and reduce comfort during human interaction. Additionally, this complex actuation system impacts reliability by increasing the vulnerability to leakages. These disadvantages limits their ability to replicate the complex, distributed deformations seen in natural muscles.

Therefore, a simplified AM system architecture is needed, which can be achieved by encoding complex deformation behavior into the actuator's embodiment. This approach aligns with the embodied intelligence (EI) framework, which emphasizes that intelligent behavior can emerge from the coupling between morphology, material properties and their interaction with the environment [11–14]. Therefore reducing the required computational load. By tailoring local interactions between the McKibben AM's braided sleeve and inner bladder, we achieve global shape change through passive, geometry-encoded actuation. In the present work, the local interaction between the braided sleeve and the compliant bladder will be employed to define the global deformation of the McKibben AM. This results in complex motions like bending or twisting emerging from a single, simple input like inflation. Currently, different strategies have been used to manufacture McKibben AMs embedding a locally adapted sleeve. These usually entail alternative manufacturing techniques, such as 3D printing or molding [15–17]. These techniques involve advanced manufacturing facilities, custom-made instruments, high material costs, low production scalability or time-consuming processes, which reduce their applicability. Alternatively, Connolly et al. [18] demonstrated a related approach using fiber-reinforced pneumatic actuators that embed complex motions by locally varying fiber orientations within a molded silicone body. While they show comparable motions as McKibben AMs, their underlying working principle differs. In the design by Connolly et al. [18], the deformation is governed by locally varying stiffness and material anisotropy, whereas McKibben AMs rely on sliding and rotation of fibers within an external braided sleeve. The McKibben architecture outstand molding-based

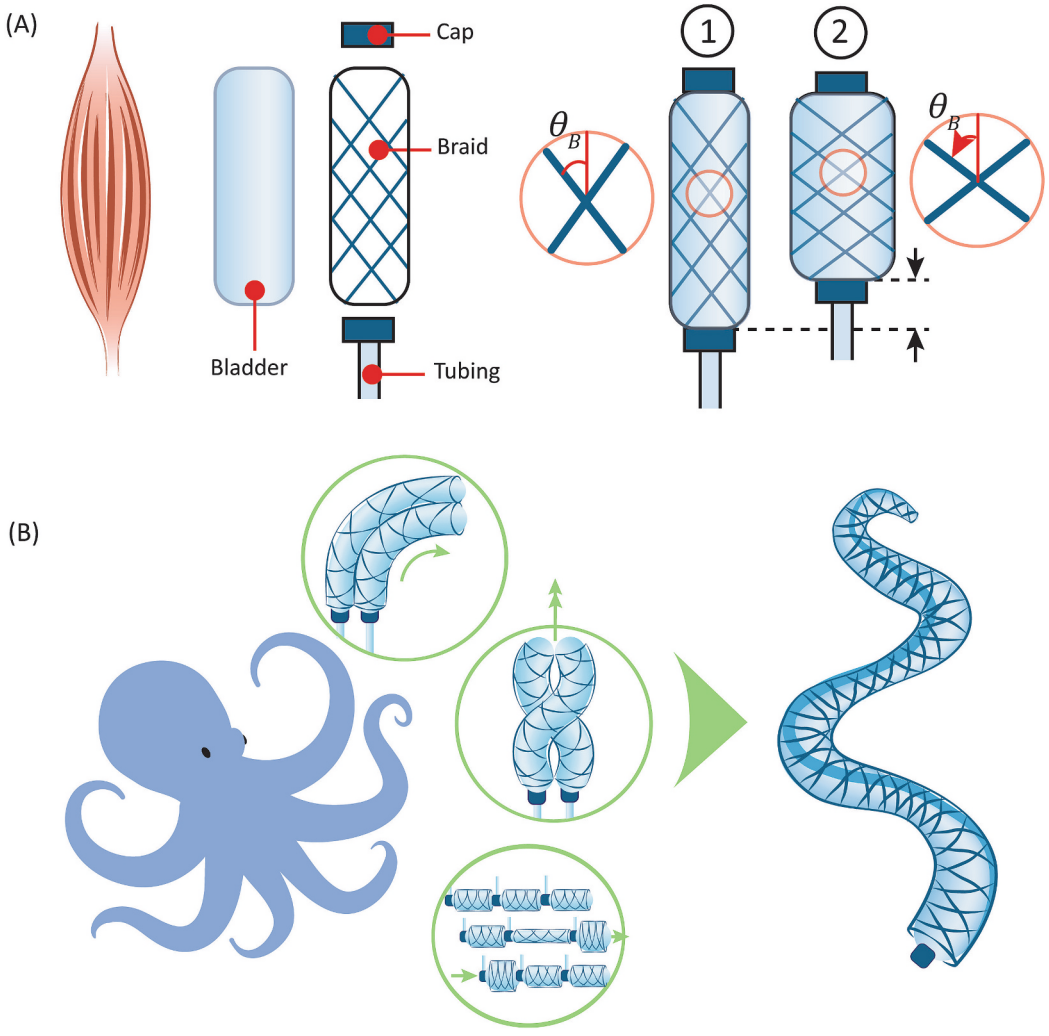

Fig. 1. McKibben Artificial Muscles (AMs). (A) Schematic representation of a McKibben Artificial Muscle (AM). Expansion of the inner bladder results in contraction or extension of the actuator, depending on the braiding angle θ_B. (B) Soft robots that embed complex motions, such as bending, twisting and advanced linear deformation, usually require a complex system of multiple McKibben AMs. To simplify robotic systems, complex motions need to be embedded in the design of a single McKibben AM.

embedding of fibers in terms of manufacturing scalability. The use of commercially available braiding machines enables efficient fabrication of actuators with greater lengths, diameters, and production throughput. To our knowledge, no McKibben AMs with locally adaptable sleeves have yet been developed while maintaining the simplicity and scalability of conventional braiding techniques.

The goal of this study is to develop embodied intelligent McKibben AMs, whose global behavior is physically programmed into their embodiment. While maintaining compatibility with regular braiding techniques, this study analyzes the relevant design parameters for functionally encoded sleeves, develops novel braiding strategies for manufacturing and evaluates the deformation behavior of prototyped mechanically encoded McKibben AMs.

2. Braiding for intelligent sleeves

2.1. Braiding for linear motion

2.1.1. Relevant design parameters

Depending on the design parameters of the braided sleeve, the interaction between the sleeve and the inflated bladder results in a specific linear motion. Therefore, knowing which parameters are relevant is essential to embed a complex linear deformation profile into the braid. This way, a singular McKibben AM can be created showing locally different contraction or extension behavior. The single AM could, for example, be implemented to exhibit complex linear locomotion [9,10] or might be wrapped such that its deformation resembles a human heart [19].

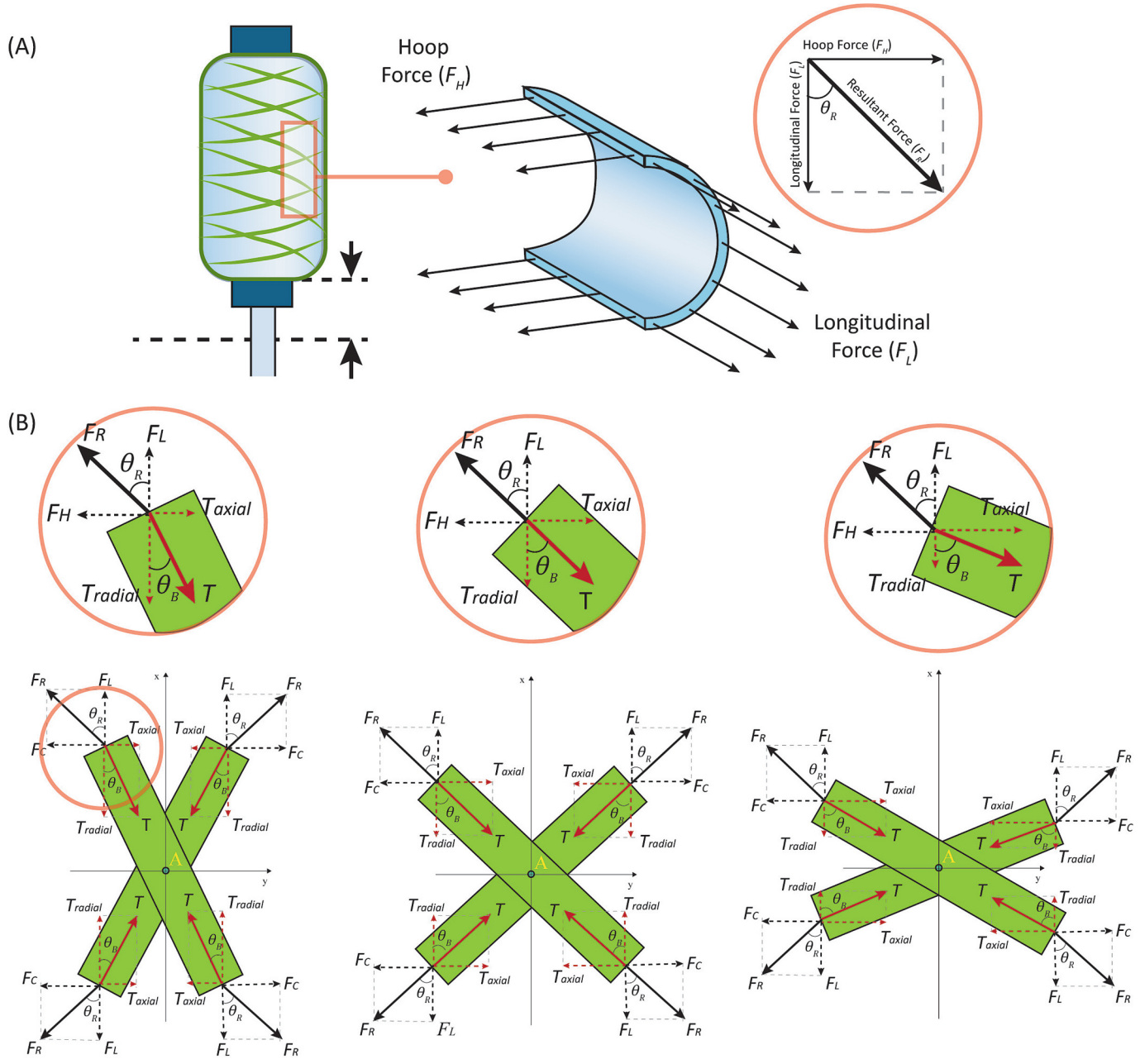

Fig. 2. How the braid angle (θ_B) determines linear motion. (A) A hoop force (F_H) and longitudinal force (F_L) are applied to the bladder during inflation, of which the resultant force (F_R) affects the braid wires, with angle θ_R. (B) Left: A braiding angle (θ_B) smaller than the resultant angle (θ_R) leads to inwards rotation of the braid wires, meaning contraction. Middle: A braiding angle (θ_B) similar to the resultant angle (θ_R) leads to no linear motion. Right: A braiding angle (θ_B) larger than the resultant angle (θ_R) leads to outward rotation of the braid wires, meaning extension.

To understand how to adjust these design parameters, we look closely into the interaction between the bladder and the braided sleeve during inflation. As shown in Fig. 2A, the inflation pressure P applied to the inner bladder of the McKibben AM results in a longitudinal force (F_L) and a circumferential force (also known as the hoop force) (F_H). They depend on the diameter D and the length L of the bladder, as elaborated in Appendix A.

In the case of an equilibrium condition, which means no linear motion, the resultant force (F_R) caused by the hoop force and longitudinal force is in line with the tension force (T) applied to the braid wires. Here, the angle of the resultant force (θ_R) is similar to the braid angle of the wires (θ_B), called the neutral angle. As described in classical hose theory [20], this neutral angle has a theoretical value of 54.7°, with its derivation provided in Appendix A.

As shown in Fig. 2B, a braid angle smaller than the neutral angle will force the wires to rotate inwards, resulting in the contraction of the McKibben AM. Similarly, a braid angle larger than the neutral angle will force the wires to rotate outwards, resulting in the extension of the McKibben AM. The amount of extension or contraction (ε) can be determined by (2), depending on stroke length (ΔL), the initial length (L_0) and the initial braiding angle (θ_{B0}). Here, a positive value indicates extension and a negative value indicates contraction.

$$\varepsilon = \frac{\Delta L}{L_0} = 1 - \frac{\cos(\theta_B)}{\cos(\theta_{B_0})} \tag{2}$$

To conclude, the linear deformation profile of the McKibben AM can be directly adapted by adjusting the braiding angle locally ($\theta_{B,i}$). The overall strain of the AM (ε_{tot}) is the result of the combined strain contributions from each local segment (ε_i), as shown in (3), (4) and (5). It should be noted that the final braiding angle after linear deformation is not solely determined by geometry, but is also influenced by external factors such as load, fiber pre-tension and actuation pressure.

$$\varepsilon_i(\theta_{B_i}) = \begin{cases} < 0, \theta_{B,i} < 54.7^\circ \\ = 0, \theta_{B,i} = 54.7^\circ \\ > 0, \theta_{B,i} > 54.7^\circ \end{cases} \tag{3}$$

$$\Delta L_{tot} = \sum \Delta L_i = \sum \varepsilon_i \bullet L_{0i} \tag{4}$$

$$\varepsilon_{tot} = \frac{\Delta L_{tot}}{L_{0,tot}} = \frac{\sum \varepsilon_i \bullet L_{0,i}}{\sum L_{0,i}} \tag{5}$$

2.1.2. Manufacturing technique

To embed a complex linear motion in a McKibben AM, a manufacturing technique had to be developed to adapt the braiding angle of the braided sleeve locally. A key objective was to retain the use of conventional braiding technology to preserve manufacturing simplicity, which can be achieved in several ways. Conventional braiding the sleeve of the McKibben AM often involves an industrial braiding machine, also known as a *Maypole braider*. This machine manufactures the braided sleeve by interlacing a set of wires around a

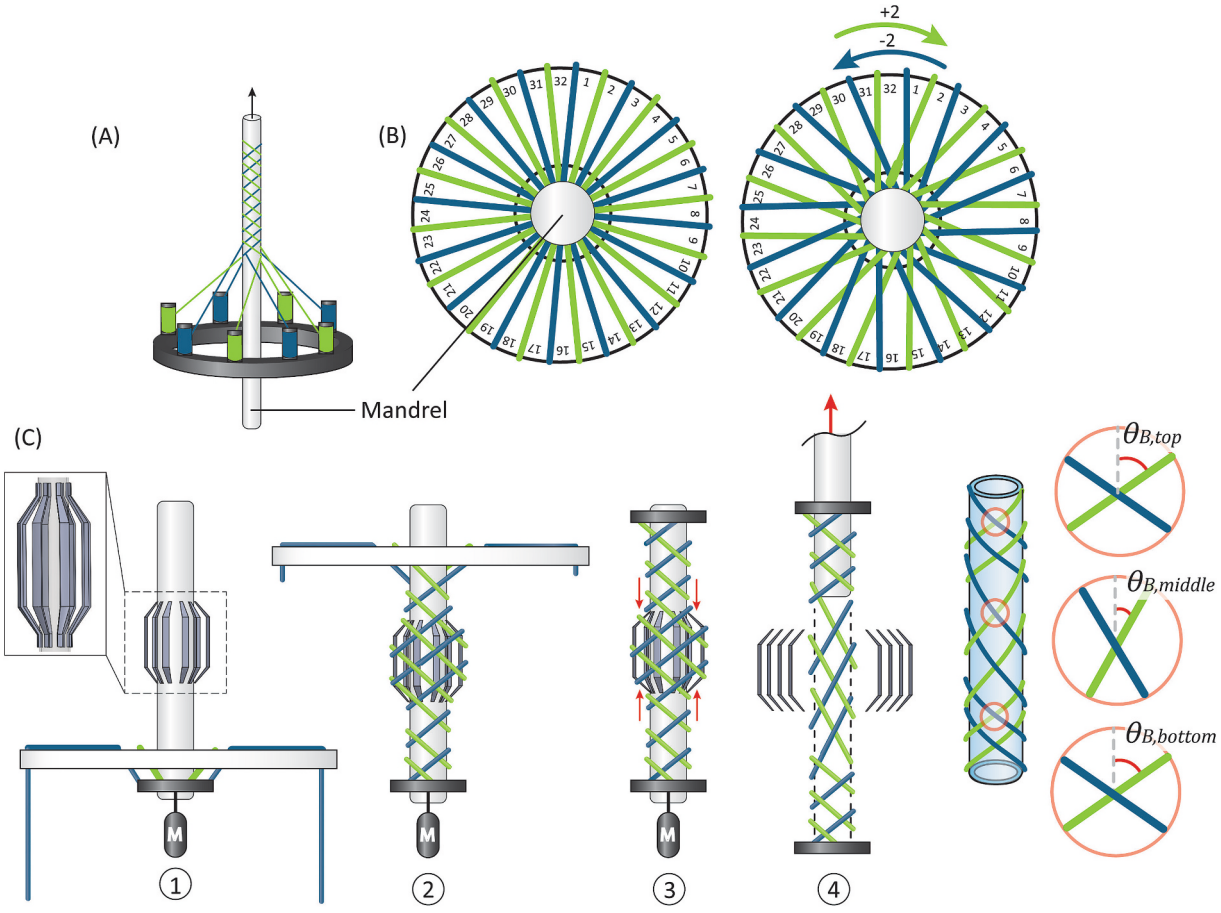

Fig. 3. Manufacturing process of a braided sleeve with a locally adaptive braiding angle. (A) A hollow round braid created around a mandrel using a conventional braiding machine. The mandrel is pulled at a constant speed for consistent braid parameters. (B) Braiding pattern using a Kumihimo braiding disc to create a hollow round braid around a mandrel. (C) Final manufacturing process. (1) Setting up the braiding disc with 32 wires attached to a cap (black) and a mandrel with sets of compliant rods (grey) to increase its diameter locally. A weight, indicated by M, introduces a constant pulling speed. (2) The wires are consistently braided around the mandrel. (3) The compliant rods are detached from the mandrel and removed from the braid by pushing them inwards. (4) The mandrel is removed from the braid, resulting in a braided sleeve with a locally adjusted braiding angle.

cylindrically shaped braiding mandrel. Normally, this mandrel has a constant diameter and is pulled at a constant speed (Fig. 3A). Interestingly, the design of the mandrel offers many opportunities to customize the braiding angle of the sleeve locally. Specifically, a locally adjustable braiding angle can be achieved by either locally adjusting the pulling speed or the diameter of the mandrel. Here, increasing the speed or increasing the mandrel diameter reduces the final braiding angle, while decreasing the speed or decreasing the mandrel diameter enlarges the final braiding angle.

Three prototypes were made to demonstrate the effect of different braiding angles over the length of a single McKibben muscle. To ease prototyping, a traditional Japanese *Kumihimo* braiding disc was used as an alternative to an industrial braiding machine. This braiding disc functions as a perfect tool to quickly iterate with the design parameters of the braided sleeve. The braiding pattern for a hollow round braid, also known as *Naiki Gumi*, was used to manufacture the braided sleeve. Fig. 3B illustrates the steps of this braiding pattern, which results in a similar braid as produced by an industrial braiding machine.

In this study, we chose to adapt the braiding angle of the sleeve by employing a mandrel with customized diameter, as this gave more consistent results in combination with the manual braiding process. The manufacturing process is shown in Fig. 3C. The mandrel was 3D-printed (*Ultimaker S5, Polylactic Acid (PLA)*) with sets of compliant rods to increase the diameter locally. The rods were attached to the mandrel by sliding their ends into circularly arranged slots embedded in the mandrel. After braiding, these rods were easily disassembled by pushing them inwards, after which the mandrel was easily removed from the braided sleeve. The diameter of the large mandrel sections was 26.5 mm, while the diameter of the small mandrel sections was 11 mm. The braid consisted of 32 polyethylene (PE) wires with a 0.3 mm diameter (*Grappler 8, Shimano*). To finish the McKibben AM, the mandrel was replaced by a silicone bladder (*Ecoflex 0030, Smooth-On*) with a similar diameter. The silicone bladder was covered by talcum powder (*Zwitsal*) to reduce the friction between the bladder and the braided sleeve, optimizing the deformation of the sleeve.

Three prototypes were manufactured, each divided into three segments meaning three customized mandrels were used. This allowed for deformation profiles with three distinct configurations. Table 1 shows the fabrication parameters of the three actuators. Note that the large mandrel sections include transition lengths of 10 mm to transition from a small diameter (11 mm) to a large diameter (26.5 mm), and the other way around. The braiding angles of the individual segments were measured using a digital microscope (*Dino-Lite Edge AM73915MZTL*), providing high magnification and resolution. The angle was determined by digitally marking the individual wires and calculating the angle between them using the DinoCapture 3.0 software. The first prototype consists of a contracting middle segment surrounded by two extending segments (Fig. 4A). The braiding angles of the top, middle and bottom segments are 57.1°, 22.5° and 57.0°, respectively. The second prototype consists of an extending middle segment surrounded by two contracting segments (Fig. 4B). The braiding angles of the top, middle and bottom segments are 35.0°, 55.8° and 34.0°, respectively. The third prototype acts as a reference, with three contracting segments (Fig. 4C). The

Table 1
Fabrication parameters of the linear actuators.

		Actuator 1	Actuator 2	Actuator 3
Top segment	Mandrel length [mm]	50	50	50
	Mandrel diameter [mm]	11	26.5	11
Middle segment	Mandrel length [mm]	50	50	50
	Mandrel diameter [mm]	26.5	11	11
Bottom segment	Mandrel length [mm]	50	50	50
	Mandrel diameter [mm]	11	26.5	11

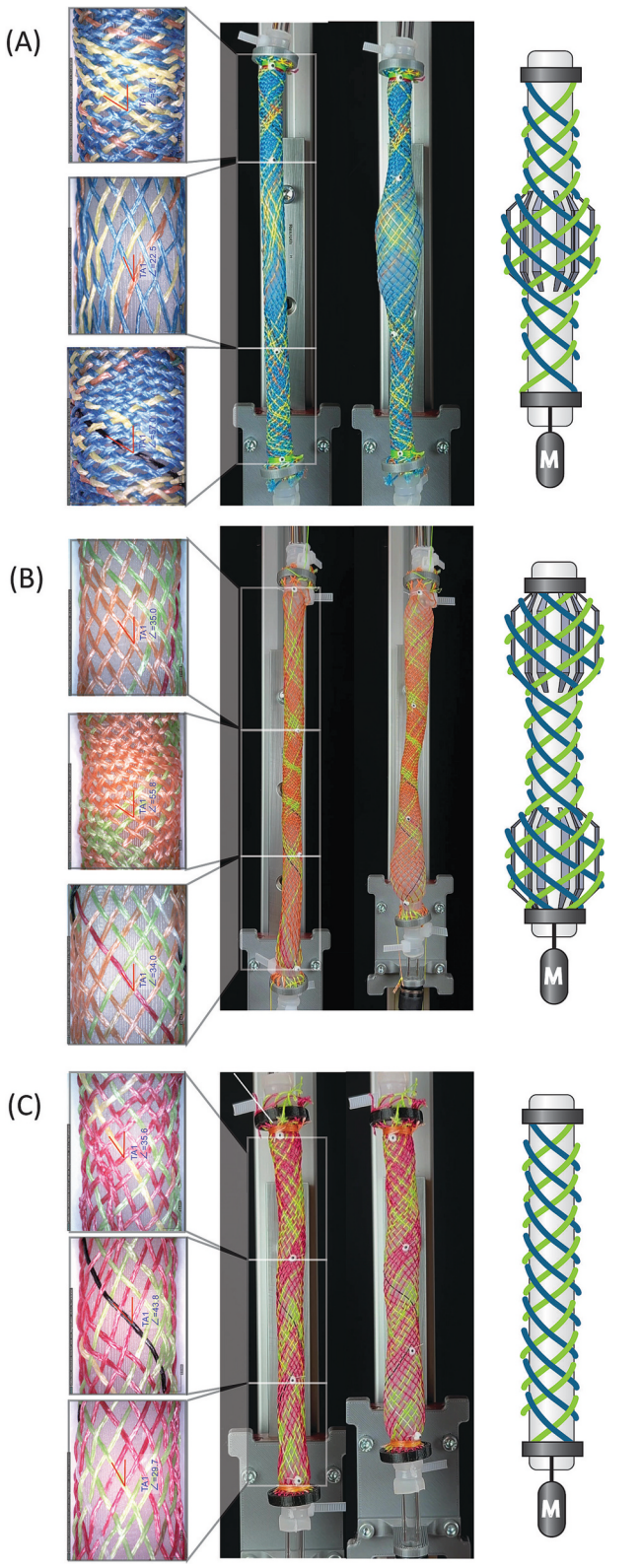

Fig. 4. Final prototypes. (A) Actuator 1 consisting of contracting middle segment surrounded by two extending segments. Right: Customized mandrel design. (B) Actuator 2 consisting of an extending middle segment surrounded by two contracting segments. Right: Customized mandrel design. (C) Actuator 3 consisting of three contracting segments, functioning as reference. Right: Customized mandrel design.

braiding angles of the top, middle and bottom segments are 35.6°, 43.8° and 29.7°, respectively. Here, it is important to remember that braiding angles below 54.7° result in contraction and braiding angles above 54.7° result in extension. The prototypes demonstrate that locally varying braiding angles can be implemented using a customized mandrel with varying diameters.

2.2. Braiding for twisting motion

2.2.1. Relevant design parameters

Currently, a single McKibben muscle can only exhibit a twisting motion in combination with other McKibben muscles or by wrapping the AM into a space-inefficient configuration. A space-efficient twisting McKibben AM would be beneficial in, for example, biomedical applications or unstructured environments [21]. To develop a McKibben artificial muscle capable of twisting, it is necessary to create an imbalance between the forces generated by the opposing helical families in the braided sleeve. The braided wires are arranged in both clockwise and counterclockwise helical patterns around the inner bladder. By altering the mechanical influence of one family relative to the other, a net torque is produced, causing the actuator to twist. For simplification, Fig. 5A illustrates how single-directional helices induce a twisting motion. When the bladder inflates, the helices expand in diameter. Because the helix wire is inelastic, this expansion is compensated by reducing the number of turns of the helix, resulting in a twisting motion. However, in traditional McKibben AMs, the clockwise and counterclockwise helices generate opposing torques that cancel each other out. Therefore, to achieve a net twisting effect, the helices must be designed asymmetrically, meaning they have a different number of turns.

Suppose we have two helical families, Helix 1 with N_1 turns and Helix 2 with N_2 turns. The total length of each helix before expansion (S_i) and after expansion (S_i') is determined using (6)-(7). Here, p_i is the helix pitch length before expansion, p_i' is the helix pitch length after expansion, D is the diameter, D' is the diameter after expansion and N_i' is the helix number of turns after expansion (Fig. 5B).

$$S_i = N_i\sqrt{p_i^2 + (\pi D)^2} \tag{6}$$

$$S_i' = N_i'\sqrt{p_i'^2 + (\pi D')^2} \tag{7}$$

Due to the inelasticity of the helices, the total helix length remains unchanged after expansion. The net twisting effect in turns (ΔN) is given by (8). The twisting angle θ_{twist} is given by (9). Here, N_i' denotes the effective continuous number of turns of each helical family after inflation. The helical number of turns after expansion is further derived in Appendix A.

$$\Delta N = N_1' - N_2' \tag{8}$$

$$\theta_{twist} = 360^\circ \bullet \Delta N \tag{9}$$

In conclusion, a single twisting McKibben AM can be created by adapting the opposing helices' number of turns (N). This means, at the same time, that the braiding angle of the clockwise helices ($\theta_{B,1}$) differs from the braiding angle of the counterclockwise helices ($\theta_{B,2}$) (Fig. 5C).

$$\theta_{twist} = \begin{cases} \neq 0, N_1 \neq N_2 and \theta_{B,1} \neq \theta_{B,2} \\ = 0, N_1 = N_2 and \theta_{B,1} = \theta_{B,2} \end{cases} \tag{10}$$

With this minor adaptation of its sleeve design, a McKibben AM can embed torque during its motion. It should be noted that Eq. (9) provides the geometric relation between the current braid configuration and the actuator twist. However, the braid geometry itself is pressure-dependent. This means the helical number of turns N_i' evolves with actuator deformation, which is governed by the internal pressure. Consequently, the twist develops continuously during inflation. The two helical families are mechanically coupled and the actuator reaches a stable twist angle when the torques from both helical families balance.

2.2.2. Manufacturing technique

A manufacturing strategy was implemented to create a disbalance in the number of turns between the opposing helices of a braided sleeve, as shown in Fig. 5D. Again, the *Kumihimo* braiding disc was employed to manufacture the braided sleeve. This time, the sleeve was braided around a regular mandrel with a constant diameter. After finalizing the sleeve and assembling the silicone bladder (*Ecoflex 0030, Smooth-On*), one helical family was tensioned. Tensioning the clockwise turning helices results in a clockwise twisting McKibben AM when pressurized. Vice versa, if the counterclockwise helices are tensioned, this results in a counterclockwise twisting McKibben AM. Introducing a difference in the number of turns (N) between the helices simultaneously means that the helices employ a different braiding angle. Table 2 shows the geometric fabrication parameters of the twisting AM.

Fig. 5E shows the final prototype with a difference in the number of turns (N), and thus a braiding angle difference. The difference in the braiding angle of the opposing helices was measured using a digital microscope (*Dino-Lite Edge AM73915MZTL*). The angle was determined by digitally marking the individual wires and calculating the angle between them using the DinoCapture 3.0 software. The disbalance was introduced by tensioning one set of helices of the prototype. To demonstrate the effect of asymmetry in the helical structure on the twisting effect, the prototype was adapted to embed a range of braiding angle differences. Using a single prototype ensured that all other design parameters of the McKibben AM remained constant, isolating the effect of the braiding angle difference. This variation was achieved by stretching the prototype, thereby decreasing the braiding angles of both helical sets. Because the helices start with different angles, their change in angle during stretch is not uniform, resulting in an increased braiding angle difference as the prototype is stretched. The McKibben AM is stretched by applying a weight of 50 g, 100 g, 150 g and 200 g. This resulted in a difference in the braiding angle ($\Delta\theta_B$) of 45.9°, 47.2°, 50.4° and 51.3°, respectively. The difference in braiding angle without using a weight was measured as 38.6°. The prototype demonstrates that by tensioning helices, their braiding angle can be adjusted compared to the opposing-turning helices.

3. Experiments

The main goal of the experiments was to investigate the effect of an adjustable braiding angle on the (1) linear motion and (2) twisting motion of McKibben AMs. Therefore, two experiments were performed, the first focusing on the linear motion and the second focusing on the twisting motion. The aim was to investigate the overall actuation behavior of the prototyped McKibben artificial muscles, to verify whether local modifications in braid parameters lead to the expected deformation responses.

3.1. Experimental Setup: Linear motion

The setup for demonstrating the linear AMs is illustrated in Fig. 6A. In this setup, the three prototypes described in Section 2.1.2 were investigated. Each prototype consisted of three segments, namely top, middle, and bottom, distinguished by their braiding angles. Four polystyrene markers were stitched onto each McKibben AM to indicate the transition between these segments. The McKibben AM was positioned vertically by clamping the proximal end onto the main frame. The distal end was attached to a vertical miniature ball runner guide (Rexroth, MWA-020-SNS-C0-H-3) by a 3D-printed support, constraining the actuator to a 2D plane and preventing out-of-plane motion. The McKibben AM was connected to a manual pump with a pressure sensor in between (IFM electronic, PU5404). The motion of the AM was recorded by a camera on a tripod, positioned approximately 40 cm in front of the actuator. The pressure sensor was connected to an analogue

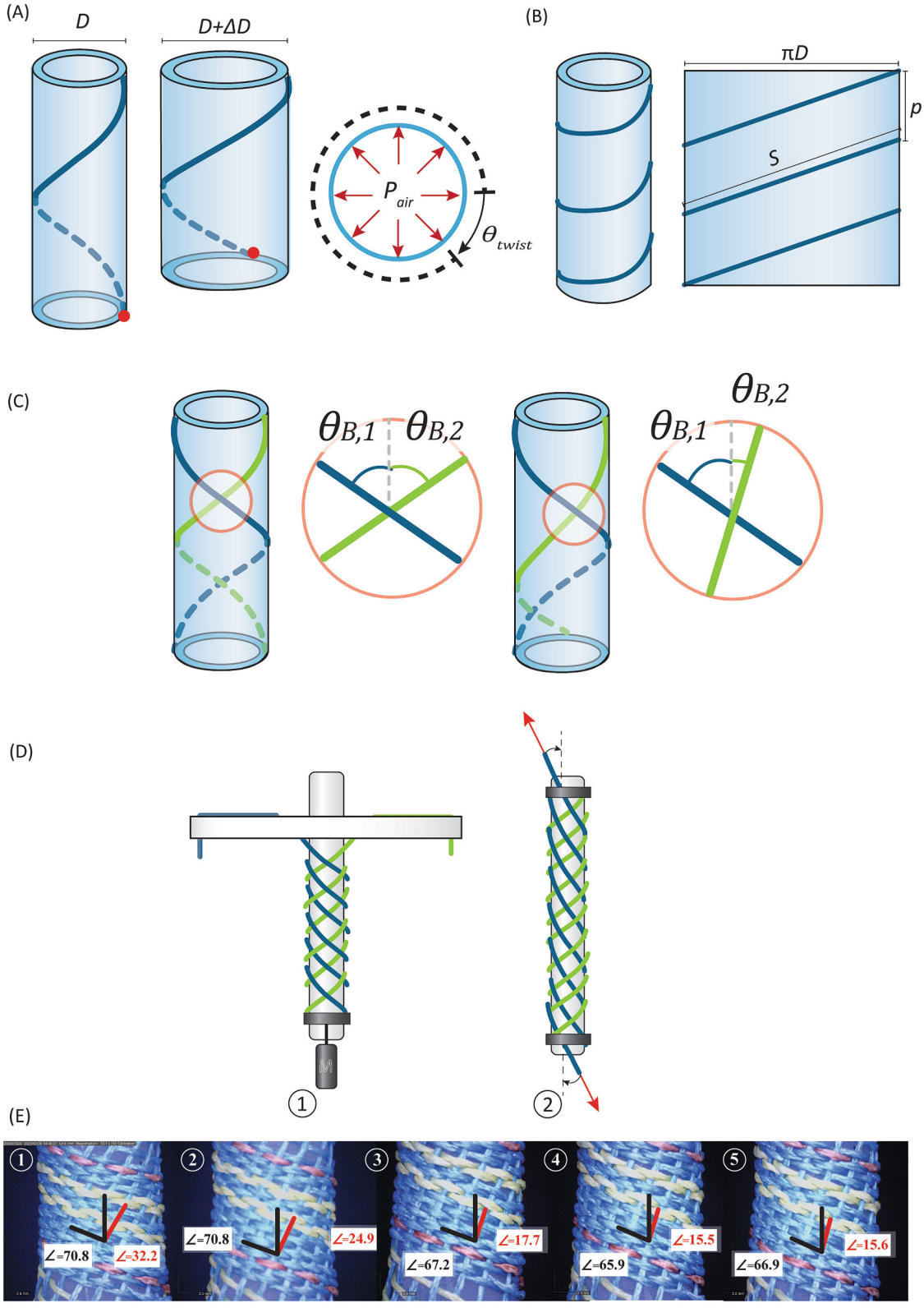

Fig. 5. Inducing a twist angle θ_{twist} by unbalanced helical families. (A) Schematic representation of twist by a single helical family. Here, D is the diameter and P_{air} is the internal pressure. (B) Helical design parameters, here p is the helical pitch length and S is the length of one helical turn. (C) Left: Balanced helical families, with similar number of turns (N) and braiding angle (θ_B), resulting in no net twisting motion. Right: Unbalanced helical families, with different number of turns (N) and braiding angle (θ_B), resulting in a net twisting motion. (D) Schematic manufacturing process. (1) Braiding the sleeve with a Kumihimo braiding disc around a regular mandrel, (2) Tensioning the wires of one helical family, resulting in a braiding angle difference between the opposing helical families. (E) Final prototype. (1) Non-stretched, with a braiding angle difference of 38.6°, (2) stretched by a 50 g weight, resulting in a braiding angle difference of 45.9°, (3) stretched by a 100 g weight, resulting in a braiding angle difference of 47.2°, (4) stretched by a 150 g weight, resulting in a braiding angle difference of 50.4° and (5) stretched by a 200 g weight, resulting in a braiding angle difference of 51.3°.

Table 2
Geometric fabrication parameters unloaded twisting actuator.

	Helical family 1	Helical family 2
Mandrel length [mm]	70	70
Mandrel diameter [mm]	10	10
Amount of turns [-]	1	3.5

signal conditioner (CPJ RAIL, SCAIME) and a data acquisition unit set at a sampling rate of 20 Hz (NI USB-6008, National Instruments Corporation). A millimeter scale bar was placed next to the McKibben AM for calibration purposes.

The deformation of the top, middle, and bottom segments of every McKibben AM was the main performance measure. The deformation was presented as stroke length (ΔL) and strain (ε), computed by (5), meaning a positive value indicates extension and a negative value contraction. The stroke length was defined as the change in length between the markers that indicated the start and end of a specific segment. The deformation was measured for different actuation pressures, ranging from 10 kPa to 50 kPa.

At the start of each measurement, the McKibben AM was positioned with the markers facing the camera. The pressure was increased in steps of 10 kPa, 20 kPa, 30 kPa, 40 kPa and 50 kPa, which was monitored in LabVIEW 2018. The subsequent pressure steps were indicated on the video footage by an auditory signal. Ten trials per condition were performed for all three prototypes. The video footage was analysed using *Tracker (6.1.7)* software (Open Source Physics). Here, the motion of the segments was extracted by tracking the four markers. An XY axis was plotted in the software with the origin positioned at the stationary proximal end of the McKibben AM. The videos were calibrated using millimetre graph paper. Comparing the X-t plots of the separate markers resulted in the relative deformation of the intermediate segments. The

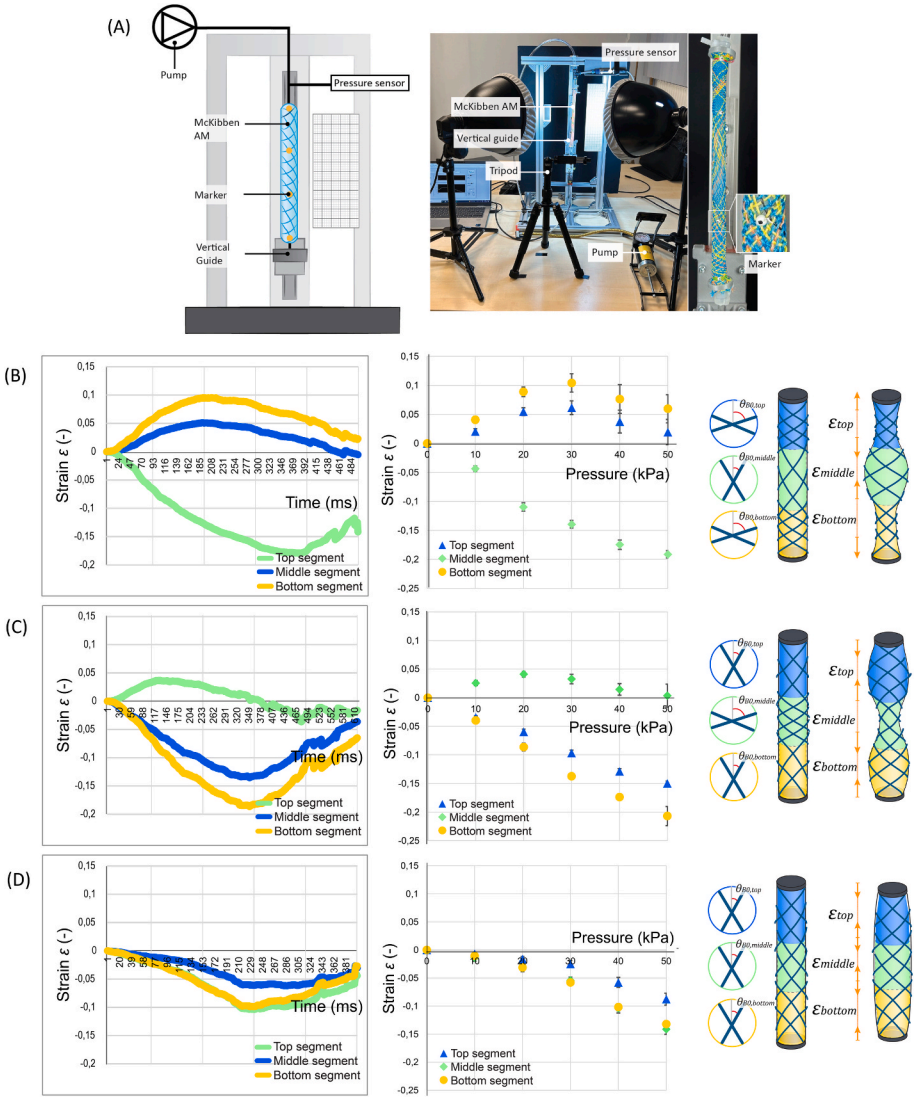

Fig. 6. Results: Linear motion. (A) Overview of the experimental setup. (B) Deformation profile of the first prototype, embedding an extending top and bottom segment and a contracting middle segment. Left: The average strain (ε) of the individual segments over time. Here, a positive strain indicates extension and a negative strain indicates contraction, showing one full actuation cycle. Right: The average strain (ε) of the individual segments for different actuation pressures. Data represent mean ± standard deviation from 10 repeated measurements (n = 10). (C) Deformation profile of the second prototype, embedding a contracting top and bottom segment and an extending middle segment. Left: The average strain (ε) of the individual segments over time, showing one full actuation cycle. Right: The average strain (ε) of the individual segments for different actuation pressures. Data represent mean ± standard deviation from 10 repeated measurements (n = 10). (D) Deformation profile of the reference prototype, embedding a contracting top, middle and bottom segment. Left: The average strain (ε) of the individual segments over time, showing one full actuation cycle. Right: The average strain (ε) of the individual segments for different actuation pressures. Data represent mean ± standard deviation from 10 repeated measurements (n = 10).

videos were recorded in 4 K resolution (3840 × 2160 pixels) at 30 fps with the camera plane perpendicular to the actuator to avoid parallax effects. The rigid scale bar was placed in the same plane as the actuator to ensure accurate pixel-to-length calibration. The small, high-contrast markers were attached to the braided sleeve with minimal contact area to reduce marker deformation. Uniform, diffuse lighting created by light boxes and a high-contrast background were used to enhance marker visibility during tracking.

3.2. Results: Linear motion

Fig. 6B–D shows the strain (ε) of the top, middle, and bottom segments of the three McKibben AMs. The first prototype has a maximum mean stroke length (ΔL) of +2.8 mm (top), −18.1 mm (middle) and +5.4 mm (bottom), corresponding to a strain of +0.06, −0.19, and +0.10, respectively. This clearly demonstrates that the middle segment, with a braiding angle of 22.5°, is contracting. Contrarily, the top and bottom segments, with braiding angles of 57.1° and 57.0°, are extending. The second prototype has a maximum mean stroke length (ΔL) of −12.2 mm (top), +2.6 mm (middle) and −15.5 (bottom), corresponding to a strain of −0.15, 0.04, and −0.21, respectively. This demonstrates that the middle segment, with a braiding angle of 55.8° is extending. Contrarily, the top and bottom segments, with braiding angles of 35.0° and 34.0°, are contracting. The third prototype has a maximum mean stroke length of −4.4 mm (top), −7.1 mm (middle) and −5.5 mm (bottom), corresponding to a strain of −0.09, −0.14, and −0.13, respectively. All three segments, with a braiding angle of 35.6°, 43.8° and 29.7°, are contracting. The actuator exhibited a full inflation–deflation cycle within approximately 0.5 s, corresponding to an estimated response time of a few hundred milliseconds. The observed dynamics are primarily governed by the compliance of the silicone bladder and the low operating pressure range used in this study.

Applying (2) to predict segment strain revealed discrepancies between theoretical and experimental values. While the model correctly predicted the direction of motion, elongation or contraction, it fell short in estimating the strain magnitude. This may be due to gradual transitions between segments, which lack sharp boundaries and introduce intermediate braiding angles not captured by the model. Additionally, the assumption of isolated segments does not reflect the mechanical interaction between adjacent segments. Despite these limitations, the theoretical framework remains valuable for understanding how braiding angles influence motion and for guiding actuator design.

3.3. Experimental Setup: Twisting motion

The setup for demonstrating the twisting AMs is illustrated in Fig. 7A. In this setup, the five prototype configurations described in Section 2.2.2 were investigated. Each configuration was created by tensioning the McKibben AM with a specific weight, inducing a corresponding braiding angle difference between the opposing helices. A nylon strap was attached to the distal end of the AM to function as a pointer. Similar to the linear motion setup, the McKibben AM was positioned vertically by clamping the proximal end onto the main frame. The McKibben AM was, again, connected to a pump with a pressure sensor in between (IFM electronic, PU5404). The rotation of the AM was recorded by a camera on a tripod positioned approximately 60 cm above the actuator. The camera was aligned with the actuator's rotation axis, fixed in position and orientation perpendicular to the measurement

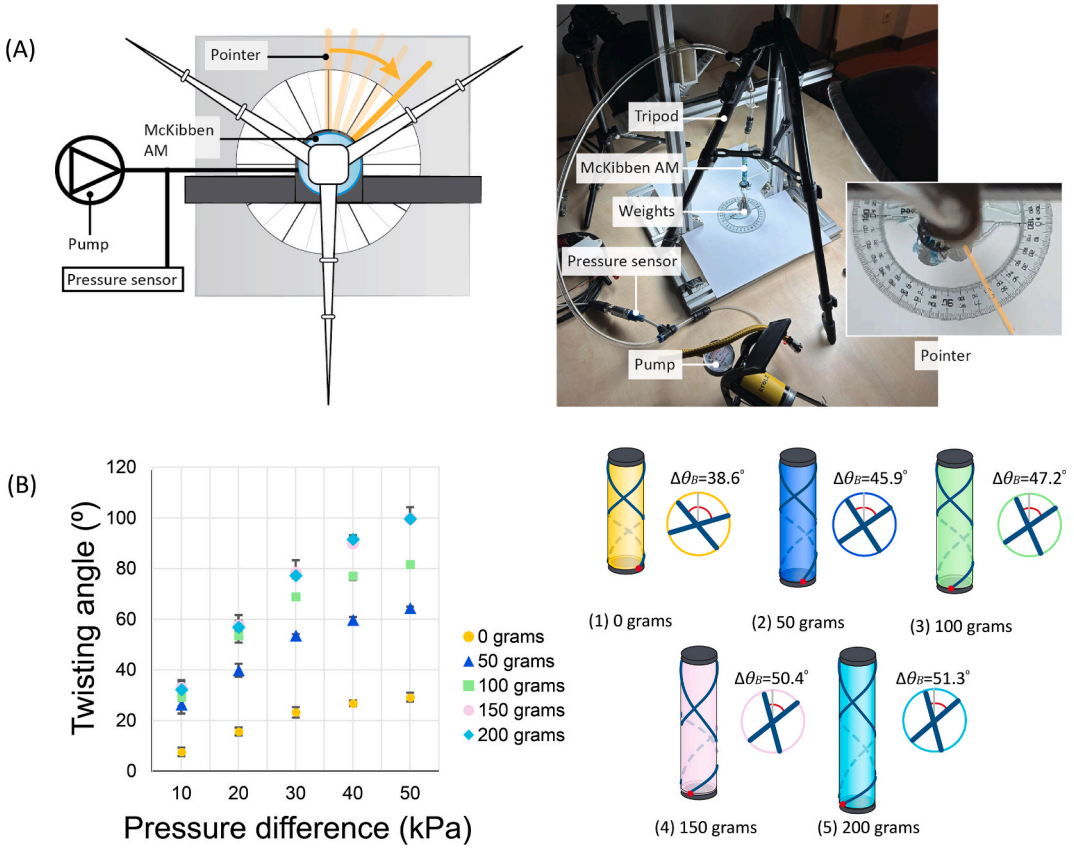

Fig. 7. Results: Twisting motion. (A) Overview of the experimental setup. (B) Twisting angle measured for different internal pressures. Data represent mean ± standard deviation from 5 repeated measurements (n = 5). Here, the final prototype is evaluated in a configuration that is (1) Non-stretched, with a braiding angle difference ($\Delta\theta_B$) of 38.6°, (2) stretched by a 50 g weight, resulting in a braiding angle difference ($\Delta\theta_B$) of 45.9°, (3) stretched by a 100 g weight, resulting in a braiding angle difference($\Delta\theta_B$) of 47.2°, (4) stretched by a 150 g weight, resulting in a braiding angle difference ($\Delta\theta_B$) of 50.4° and (5) stretched by a 200 g weight, resulting in a braiding angle difference ($\Delta\theta_B$) of 51.3°.

plane. A circular protractor was placed beneath the McKibben AM to measure the rotation. The videos were recorded in 4 K resolution (3840 × 2160 pixels) at 30 fps. Uniform, diffuse lighting created by light boxes and a high-contrast background were used to enhance pointer visibility.

The twisting angle (θ_{twist}) of the McKibben AM configurations was the main performance measure. The angle was measured for different actuation pressures, ranging from 10 kPa to 50 kPa. At the start of each measurement, the McKibben AM was positioned with the pointer facing 0 degrees on the circular protractor. The pressure was increased in steps between 10 kPa, 20 kPa, 30 kPa, 40 kPa and 50 kPa, which was monitored in LabVIEW 2018. The subsequent pressure steps were indicated on the video footage by an auditory signal. Five measurements per condition were performed for all five prototype configurations. The twisting angle was extracted from the video footage by analysing the final position of the pointer on the circular protractor.

3.4. Results: twisting motion

Fig. 7B shows the twisting angle for the different prototype configurations, depending on the actuation pressure. The maximum mean twisting angle was 29°, 64°, 82°, 100° and 100° for the prototype stretched by 0 g, 50 g, 100 g, 150 g and 200 g, respectively. A saturation in twisting angle seems to be reached when being stretched by a weight of 150 g, which resembles a braiding angle difference of 50.4°.

4. Discussion

The goal of this study was to develop embodied intelligent McKibben AMs by designing for encoded interactions between the braided sleeve and the inner bladder. In this McKibben AM design, the local interaction between the braid and bladder defines the global, complex shape transformation. This concept is inspired organisms embedding fiber-reinforced architecture, such as the octopus. The octopus controls the shape of its arms through distributed motions such as contraction, extension, twisting, and bending. In the octopus, contraction, extension, and twisting are driven by longitudinal, circular, and helical muscles, respectively. Bending arises from the coordinated interaction of these muscles. Similarly, in the McKibben AM, linear motion and twisting were directly programmed, and bending can emerge from a combination of these linear motions.

As the design parameters of the braided sleeve are key for shaping the deformation profile of the McKibben AM, the braided sleeve was designed such that its local adaptations caused complex motions. The braiding angle between the wires was identified as the core parameter to embed multiple motions in the sleeve. First, the braiding angle defines whether the AM is contracting or extending upon inflation, and additionally the range of extension or contraction. Lowering the braiding angle beyond 54.7° results in local contraction, whereas increasing the braiding angle beyond 54.7° results in local extension. A controlled change in braiding angle along the length of the braided sleeve was achieved by introducing a customized mandrel in the braiding process. Here, a mandrel with increased diameter results in a reduced braiding angle, and a decreased mandrel diameter results in an increased braiding angle. Secondly, a twisting motion can be embedded into the braided sleeve by introducing a differential in the number of turns between the opposing helical families. This results in a braiding angle difference between those wires. This disbalance was achieved by simply tensioning one helical family.

Experiments showed that the local adaptation of a McKibben AM's braiding angle successfully resulted in complex deformation profiles. McKibben AMs were prototyped using the beforementioned strategies for local braiding angle adjustment. The segments with braiding angles larger than 54.7° effectively caused local extension, whereas segments with smaller braiding angles caused local contraction. Since 54.7° represents the neutral angle, the available range for extension is inherently smaller than that for contraction. This was also reflected in the experiments, where the mean length shifts of the extending segments were consistently lower than those of the contracting segments. The largest measured difference within a single McKibben AM was found between segments with a braiding angle of 57.1° and 22.5°, with a relative maximum strain (ε) of +0.06 and minimum strain of −0.19. Interestingly, the strain of the extending segments decreased at higher pressure levels. This reduction may be attributed to the curvature observed in the McKibben muscle under high pressure, likely caused by internal structural irregularities, or by the static friction of the linear guide. While the exact mechanism was not investigated in this study, these effects highlight areas for further systematic investigation in future work. Additionally, a difference between inflation and deflation cycles was observed, indicating the presence of mechanical hysteresis. This is a well-known characteristic of McKibben actuators and other soft pneumatic systems. The hysteresis primarily arises from the viscoelastic behavior of the silicone bladder and frictional energy losses between the internal bladder and the braided sleeve.

A twist motion was successfully induced by creating a disbalance between the braiding angle of the opposing helical families. A braiding angle difference of 50.4° resulted in the largest twist angle, 100 degrees, using an actuation pressure of 50 kPa. The experiments showed that the twisting angle of the actuator saturates at a certain pressure, depending on the braiding angle difference. This behavior is expected, as the actuator continues to twist until the torque generated by the opposing helical family is balanced, effectively aligning toward a braiding angle difference of 0 degrees. Theoretically, the maximum possible braiding angle difference approaches 90°, with one set of helices nearing a braiding angle of 0° and the other approaching 90°. However, in the prototyped actuator, saturation occurred at a difference of 50.4°, likely due to geometric constraints and internal friction.

Bending in the McKibben AM can be locally encoded into the braid by combining contraction and extension patterns. A McKibben AM incorporating an extending leg and a contracting leg was prototyped as a proof of concept. This segment was built into a modular AM to showcase different local motion modules can be embedded along the length of the actuator, including contraction/extension sequences, a bending module, and a twisting module. This modular composition highlights the potential of how complex, global shape changes arise from local braid-bladder interactions. Fig. 8 provides an overview of guidelines for the design of a modular McKibben AM embedding a complex deformation profile along its length. Future work will look into strategies to combine complex linear motion, bending and twisting into a monolithic non-assembly actuator, thereby focusing on a technique to tension the helical wires in a localized manner.

Future research should further explore the potential of these embodied intelligent AMs by investigating a wider range of actuation pressures, braiding angles, and wire types. The use of automated braiding machines could enable precise local adjustments while avoiding unintended structural irregularities, and also allow for more accurate measurements through synchronized data acquisition. Although care was taken to minimize camera distortion, the optical tracking measurements may still be subject to parallax errors. Future work will employ higher-precision measurement methods to further reduce uncertainty. Nevertheless, the current setup was sufficient to capture consistent and repeatable results, clearly illustrating the overall deformation trends.

Force characterization was not included in this study, as the focus was on deformation behavior rather than maximizing force output. Since the fundamental configuration of McKibben actuators remains unchanged, the local braid adaptations introduced here are not expected to significantly affect their intrinsic force-generation behavior. Future work will include quantitative testing under load to verify this.

No degradation was observed during the experimental period, the variability between cycles remained low (see Figs. 6 and 7), but long-term cyclic testing will be required to evaluate durability. Applying adhesives at wire crossover points may prevent fiber sliding and extend

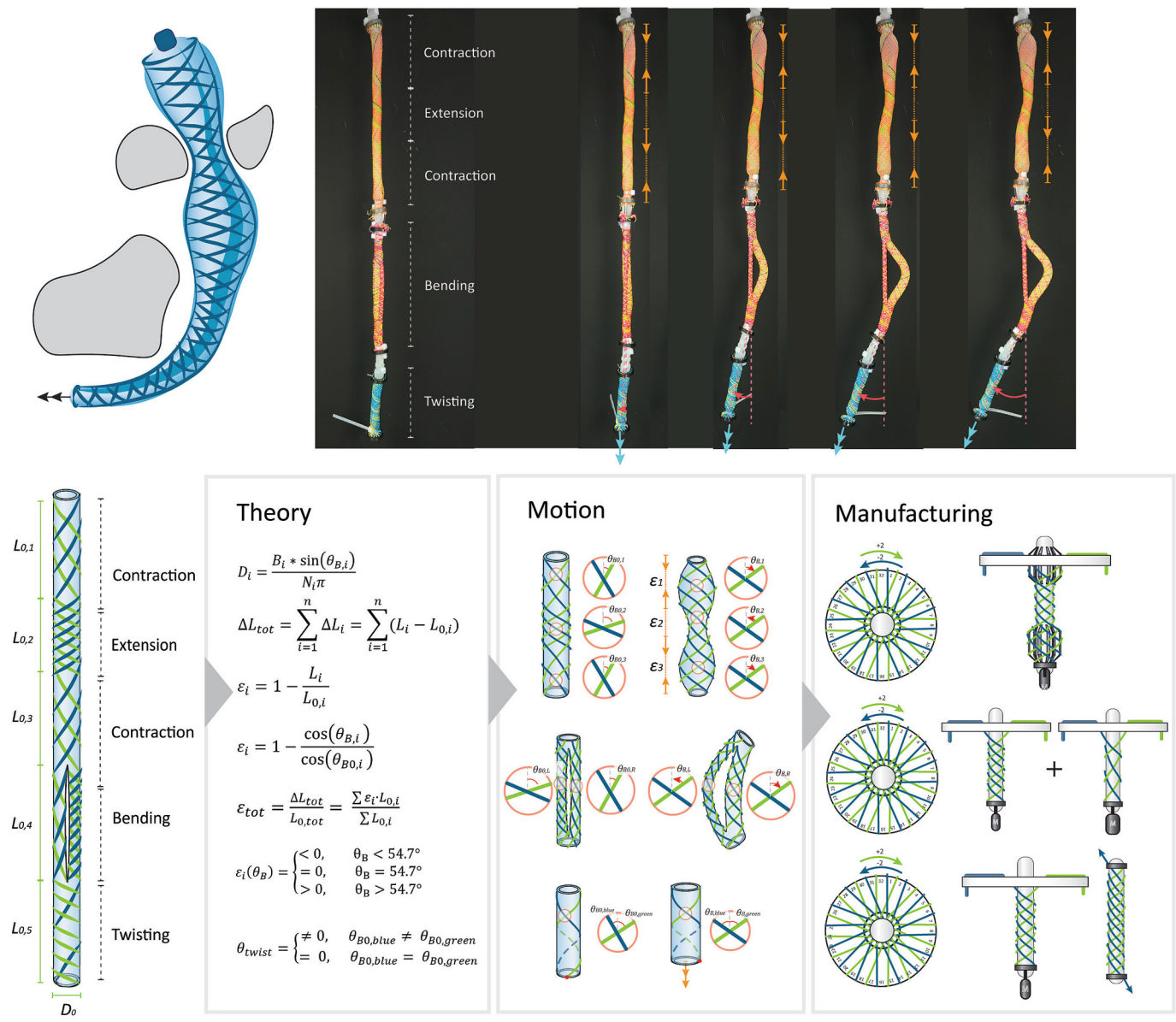

Fig. 8. Proof of concept of a modular McKibben Artificial Muscle. Top: Prototyped McKibben AM including contraction/extension sequences, a bending module, and a twisting module. Bottom: Guideline overview for the design of a modular McKibben AM for complex motion.

actuator lifetime, as demonstrated by Kobayashi et al. [22].

Alternative actuation methods, such as (electro)magnetism or temperature-driven mechanisms, could enhance the responsiveness of intelligent McKibben AMs to their environment. This opens opportunities for untethered and energy-efficient actuators. In addition, the effects of both downscaling and upscaling on the deformation profile of the AM should be assessed. The current design provides a strong foundation for scalability, as the global behavior of the McKibben AM is inherently defined by its physical structure, reducing the need for complex control systems.

Embodied intelligent AMs offer strong potential for integration into soft robotic arms that require complex deformation profiles while maintaining simple control schemes. This is particularly valuable in applications involving constrained or hard-to-reach environments. Additionally, these mechanically encoded AMs can simplify the design of soft exoskeletons and prosthetics by enabling complex movements through lightweight and low-complexity actuation. Beyond wearable robotics, the developed AMs may also be applied in bioinspired systems such as artificial organs and continuum robotic arms, where they can generate complex motions using simple inputs within a compact, space-efficient structure.

5. Conclusion

This study demonstrated that complex motion in McKibben artificial muscles (AMs) can be embedded by design, without complex control systems. Inspired by the decentralized actuation strategies of biological systems such as the octopus, we developed embodied intelligent AMs whose global deformation behavior is embedded by local interactions between the braided sleeve and the inner bladder. This highly reduces the complexity of both their actuation and system architecture, just by designing the actuator for a pre-defined motion. By tailoring the braiding angle along the actuator's length, a modular design approach within a singular McKibben AM can be deployed. Different motion types are locally embedded, such as contraction, extension, twisting and bending. This creates opportunities for the implementation of McKibben AMs in complex environments which require advanced motions and space-efficient systems, such as bioinspired artificial organs, continuum

robotic arms, wearable exoskeleton, prosthetics or surgical robotics.

Manufacturing strategies were developed that preserve the simplicity of conventional braiding techniques used in commercial McKibben AMs. As a result, material costs remain low and the production process is highly scalable. While the study used manual braiding, an industrial braiding machine (such as maypole braiders) can easily execute a similar process to reduce production time. Popular braided sleeve suppliers list product lines covering diameters ranging between 1–100 mm with lengths of several meters, showcasing the potential for scaling. Further advancements in automated braiding machines could enable precise spatial control of the braiding angle along the McKibben AM, increasing its deformation accuracy and repeatability for large-scale manufacturing. This scalability increases the potential to transfer mechanically encoded McKibben AMs from a laboratory setting into commercially implementation in real-world systems. Additionally, embedding alternative actuation methods, such as (electro) magnetism or temperature-driven mechanisms, would enhance the responsiveness of intelligent McKibben AMs even further. This enables untethered operation in mobile and wearable applications.

Implementation of these embodied intelligent AMs reduces their reliance on complex controllers or bulky multi-actuator setups. In the long term, these actuators could serve as building blocks for fully soft robotic systems with embedded intelligence, capable of responding to their environments through physical programming.

CRediT authorship contribution statement

Vera Gesina Kortman: Writing – original draft, Visualization, Validation, Methodology, Conceptualization. **Jovana Jovanova:** Writing – review & editing, Supervision. **Aimée Sakes:** Writing – review & editing, Supervision.

Declaration of competing interest

The authors declare that they have no known competing financial interests or personal relationships that could have appeared to influence the work reported in this paper.

Appendix A

The neutral angle is well-defined in classical hose theory and can be derived as follows [15]:

$$F_H = \frac{PDL}{2} \tag{A.1}$$

$$F_L = \frac{PD^2\pi}{4} \tag{A.2}$$

$$\tan(\theta_R) = \frac{F_L}{F_H} = \frac{2L}{D\pi} \tag{A.3}$$

$$L = \frac{D\pi}{\tan(\theta_R)} \tag{A.4}$$

$$\tan(\theta_R) = \frac{2}{\tan(\theta_R)} \tag{A.5}$$

$$\tan^2(\theta_R) = 2 \tag{A.6}$$

$$\theta_R = \theta_B = \tan^{-1}\sqrt{2} = 54.7^\circ \tag{A.7}$$

$$S_1 = N_1\sqrt{p_1^2 + (\pi D)^2} \tag{A.8}$$

$$S_2 = N_2\sqrt{p_2^2 + (\pi D)^2} \tag{A.9}$$

$$S_1' = N_1'\sqrt{p_1'^2 + (\pi D')^2} \tag{A.10}$$

$$S_2' = N_2'\sqrt{p_2'^2 + (\pi D')^2} \tag{A.11}$$

$$N_1' = N_1\frac{\sqrt{p_1^2 + (\pi D)^2}}{\sqrt{p_1'^2 + (\pi D')^2}} \tag{A.12}$$

$$N_2' = N_2\frac{\sqrt{p_2^2 + (\pi D)^2}}{\sqrt{p_2'^2 + (\pi D')^2}} \tag{A.13}$$

$$\Delta N = N_1' - N_2' \tag{A.14}$$

$$\theta_{twist} = 360^\circ \bullet \Delta N \tag{A.15}$$

Data availability

Data will be made available on request.

All data that support the findings of this study are included within the article (and any supplementary files).

References

[1] H. Tomori, T. Nakamura, Theoretical comparison of McKibben-type artificial muscle and novel straight-fiber-type artificial muscle, Int. J. Autom. Technol. 5 (4) (2011) 544–550, https://doi.org/10.20965/ijat.2011.p0544.

[2] H. F. Schulte and J. R. Pearson, "Characteristics of the braided fluid actuator," 1961.

[3] R. Kang, D.T. Branson, T. Zheng, E. Guglielmino, D.G. Caldwell, Design, modeling and control of a pneumatically actuated manipulator inspired by biological continuum structures, Bioinspir. Biomim. 8 (3) (2013) 036008, https://doi.org/10.1088/1748-3182/8/3/036008.

[4] E. Papadakis, D.P. Tsakiris, M. Sfakiotakis, An octopus-inspired soft pneumatic robotic arm, Biomimetics 9 (12) (2024) 773, https://doi.org/10.3390/biomimetics9120773.

[5] K. Suzumori, S. Wakimoto, K. Miyoshi, and K. Iwata, "Long bending rubber mechanism combined contracting and extending tluidic actuators," in *2013 IEEE/RSJ international conference on intelligent robots and systems*, 2013: Ieee, pp. 4454-4459, doi: 10.1109/IROS.2013.6696996.

[6] J. Zou, et al., Muscle-fiber array inspired, multiple-mode, pneumatic artificial muscles through planar design and one-step rolling fabrication, p. nwab048, Natl. Sci. Rev. 8 (10) (2021), https://doi.org/10.1093/nsr/nwab048.

[7] Z. Lin, Q. Shao, X.-J. Liu, H. Zhao, An anthropomorphic musculoskeletal system with soft joint and multifilament pneumatic artificial muscles, Adv. Intell. Syst. 4 (10) (2022) 2200126, https://doi.org/10.1002/aisy.202200126.

[8] T. Doi, S. Wakimoto, K. Suzumori, and K. Mori, "Proposal of flexible robotic arm with thin McKibben actuators mimicking octopus arm structure," in *2016 IEEE/RSJ International Conference on Intelligent Robots and Systems (IROS)*, 2016: IEEE, pp. 5503-5508, doi: 10.1109/IROS.2016.7759809.

[9] H. Sato, et al., Development of a compact pneumatic valve using rotational motion for a pneumatically driven mobile robot with periodic motion in a pipe, IEEE Access 9 (2021) 165271–165285, https://doi.org/10.1109/ACCESS.2021.3135035.

[10] Y. Mano, R. Ishikawa, Y. Yamada, and T. Nakamura, "Development of high-speed type peristaltic crawling robot for long-distance and complex-line sewer pipe inspection," in *2018 IEEE/RSJ International Conference on Intelligent Robots and Systems (IROS)*, 2018: IEEE, pp. 8177-8183, doi: 10.1109/IROS.2018.8593436.

[11] R. Pfeifer and J. Bongard, *How the body shapes the way we think: a new view of intelligence*. MIT press, 2006.

[12] C. Laschi, M. Cianchetti, Soft robotics: new perspectives for robot bodyware and control, Front. Bioeng. Biotechnol. 2 (2014) 3, https://doi.org/10.3389/fbioe.2014.00003.

[13] D. Zambrano, M. Cianchetti, C. Laschi, in: The Morphological Computation Principles as a New Paradigm for Robotic Design, University of, Zurich, 2014, pp. 214–225, https://doi.org/10.13140/2.1.1059.4242.

[14] D. Howard, A.E. Eiben, D.F. Kennedy, J.-B. Mouret, P. Valencia, D. Winkler, Evolving embodied intelligence from materials to machines, Nat. Mach, Intell 1 (1) (2019) 12–19, https://doi.org/10.1038/s42256-018-0009-9.

[15] D. Sangian, From traditional braiding methods to additive manufacturing for fabricating Mckibben artificial muscles, Biomed. J. Sci. Tech. Res 38 (5) (2021), https://doi.org/10.26717/BJSTR.2021.38.006211.

[16] W. Tian, S. Wakimoto, D. Yamaguchi, T. Kanda, Fabrication process for twisting artificial muscles by utilizing braiding technology and water-soluble fibers, IEEE Rob. Autom. Lett. 9 (4) (2024) 3147–3154, https://doi.org/10.1109/LRA.2024.3360817.

[17] S. Yahara, S. Wakimoto, T. Kanda, K. Matsushita, McKibben artificial muscle realizing variable contraction characteristics using helical shape-memory polymer fibers, Sens. Actuators, A 295 (2019) 637–642, https://doi.org/10.1016/j.sna.2019.06.012.

[18] F. Connolly, C.J. Walsh, K. Bertoldi, Automatic design of fiber-reinforced soft actuators for trajectory matching, Proc. Natl. Acad. Sci. 114 (1) (2017) 51–56, https://doi.org/10.1073/pnas.1615140114.

[19] M.A. Horvath, et al., Towards alternative approaches for coupling of a soft robotic sleeve to the heart, Ann. Biomed. Eng. 46 (2018) 1534–1547, https://doi.org/10.1007/s10439-018-2046-2.

[20] Society of Automotive Engineers Fluid Conductors and Connectors Technical Committee, "Wire Braid Angle Response Characteristics in Hydraulic Hose," *SAE Transactions,* vol. 106, pp. 107-26, 1997, doi: 10.4271/972706.

[21] T. Roche *et al.*, "Soft robotic sleeve supports heart function," *Science translational medicine,* vol. 9, no. 373, p. eaaf3925, 2017, doi: 10.1126/scitranslmed.aaf3925.

[22] R. Kobayashi, H. Nabae, Z. Mao, G. Endo, K. Suzumori, Enhancement of thin Mckibben muscle durability under repetitive actuation in a bent state, IEEE Rob. Autom. Lett. (2024), https://doi.org/10.1109/LRA.2024.3455890.